www.amlett.com, www.vbripress.com/aml, DOI: 10.5185/amlett.2015.5663 Published online by the VBRI press in 2015

Photoluminescence and photoconductivity of Ni doped titania nanoparticles

Anand Kumar Tripathi[1], Mohan Chandra Mathpal[1*], Promod Kumar[2], Vivek Agrahari[1], Manish Kumar Singh[3], Sheo Kumar Mishra[4], M. M. Ahmad[2], Arvind Agarwal[1]

[1]*Department of Physics, Motilal Nehru National Institute of Technology, Allahabad 211004, India*
[2]*Department of Physics, National Institute of Technology, Hazratbal, Srinagar 190006, India*
[3]*Department of Physics, LNM Institute of Information Technology, Jaipur 302031, India*
[4]*Department of Physics, University of Lucknow, Lucknow 22607, India*

[*]Corresponding author. Tel: (+91) 532 2271263; E-mail: mohanatnpl@gmail.com

Received: 04 September 2014, Revised: 02 November 2014 and Accepted: 12 November 2014

ABSTRACT

The Ni doped titania nanostructures were synthesized by sol-gel method followed by calcination at 400°C for one hour. The optical band gap for these nanostructures indicates the red shift. The doped TiO_2 nanostructures are spherical in shape. The pure TiO_2 exhibits all the possible emission bands while Ni doped TiO_2 nanoparticles show blue-green emission bands. The results suggest that Ni^{2+} replace some Ti^{4+} in TiO_2 lattice with tensile strain while TiO_2 remained in the form of anatase phase, reduces its band gap energy. The synthesized TiO_2 exhibits enhanced photoconducting properties. The work suggest that the titania based materials can have potential applications in photovoltaics, optoelectronic devices and photoconductors in replacement of expansive materials by controlling the compositions and morphology of the nanostructures. Copyright © 2015 VBRI press.

Keywords: Crystal structure; nanoparticles; photoconductivity; photoluminescence.

Anand Kumar Tripathi received the M.Sc. (Physics) degree from V. B. S. Purvanchal University, Jaunpur, India in 2006. He has submitted his Ph.D. thesis to Motilal Nehru National Institute of Technology, Department of Physics, Allahabad, India in 2014. He is working as faculty of physics in Devprayag Institute of Technical Studies, Allahabad, India. His research interest includes the structural, optical and photoresponse properties of metal oxide multifunctional nanomaterials.

Mohan Chandra Mathpal received his M.Phil. degree in Material Science from Annamalai University Tamilnadu, India in 2008 and M.Sc. degree in Physics from C. C. S. University, Meerut in 2006. He has submitted his Ph.D. thesis to Motilal Nehru National Institute of Technology (MNNIT), Department of Physics, Allahabad, India in 2014. His current research interest includes plasmonic metamaterials, conducting-semiconducting thin films, heterostructures, sensors, oxides nanomaterials, DMS and magnetic nanostructures, structural and optical properties of hybrid materials for superior photovoltaics applications.

Promod Kumar received his M.Tech. degree in Nanotechnology in 2010 from Guru Gobind Singh Indraprastha University, Kashmere Gate, Delhi, India. He is pursuing his Ph.D. degree in Department of Physics at National Institute of Technology, Hazratbal, Srinagar (J&K), India. He is also teaching Physics to the graduate students in the institute. His fields of the research interests are plasmonic and optoelectronics properties of metallic nanostructures and graphene based noble metal nanoclusters and composites.

Introduction

Titania (TiO_2) is the most promising catalyst for the photocatalytic applications **[1-3]**. It is effective as a photo-catalyst, highly stable against photo-corrosion, environmentally non-hazardous, and capable to absorb UV light with low quantum efficiency due to its wide energy gap (3.2 eV of anatase phase) **[1, 4]**. In addition, titanium dioxide (TiO_2) has high specific surface area, which affords extremely low photo-activity due to large number of bulk and surface defects **[2]**. However, the efficiency of TiO_2 nanoparticles for photocatalytic hydrogen production is still limited because the large energy band gap (3.2 eV of anatase phase) which permits absorption of very small part

of visible light. Other factors limiting efficiency for photocatalytic hydrogen production are recombination of electron-hole pairs at the surface instead of in bulk, and poor crystallinity of TiO_2 nanoparticles **[1, 2]**. Due to large energy band gap of TiO_2, input energy greater than 3.2 eV is required to excite an electron from the valence band to the conduction band. Many efforts to modify the band gap and photoresponse properties of TiO_2 have been initiated to improve stability, reduce the energy band gap and enhance the photocatalytic rate. These efforts include the loading of the noble and non-noble surface metals, adding a photosensitizer, changing the preparation method and incorporating nanoparticles into the interlayer of the photocatalysts **[1, 2, 4-7]**. In order to use TiO_2 for solar energy more efficiently, most of the investigations are focused on the preparation of TiO_2 which is sensitive to visible light. There are several ways for improving the performance of titania photocatalysts such as doping of the elements. The structural, optical and photoconductivity properties of Ag, Sn, Mn doped TiO_2 based materials have been already discussed in details **[5-9]**. Nickel has been found to be an efficient non-noble metal for improving the photocatalytic activity **[8-10]**. Jing et al. reported that a Ni-doped mesoporous TiO_2 catalyst plays an important role in improving thermal stability and controlling the morphology of mesoporous photocatalysts **[2]**. The p-type conducting behavior was also occasionally observed for TiO_2 after doping with certain metal ions such as Fe^{3+}, Co^{3+}, Ni^{2+}, Cu^{1+} **[11-19]**. The change of semiconducting behavior has been attributed to the hetero-unions formed between n-type TiO_2 and p-type metal oxide dopant **[17]**. Among various transition metal ion dopants, Ni^{2+} appears to be a more efficient dopant for TiO_2 as it has improved the photocatalytic activity of certain semiconductor photocatalysts **[20, 21]**. The reason for this enhancement has been tentatively attributed to the suppression of recombination of electron-hole pairs on the surface of the TiO_2 catalyst by low valence Ni^{2+} ions **[22]**. In another study, Devi et al. evaluated the photocatalytic activity of 0.08% Ni^{2+}-doped TiO_2 powders by degrading methyl orange (MO), an azo dye, under solar light and found considerable activity for this reaction **[23]**. This improved activity has been attributed to the enhanced separation of photo-generated electron-hole pairs due to the presence of Ni^{2+} ions in TiO_2. In the present paper different amounts of Ni-doped TiO_2 powders were prepared and the effects of doping on structural, optical, photoluminescence and photoconductivity behavior of TiO_2 have been investigated.

Experimental

Materials and methods

Titanium tetra isopropoxide (TTIP), ethanol and $NiCl_2.6H_2O$ were used (Analytical grade) for the preparation of samples. These AR grade chemicals were purchased from Merck. Sol-gel method was used to synthesize the undoped and doped TiO_2 nanoparticles. The mixture of titanium tetra isopropoxide (TTIP) and ethanol was taken as main precursor. As a dopant precursor, 5 gm of $NiCl_2.6\ H_2O$ was dissolved in 100 ml of distilled water which leads 0.0123 gm of Ni in 1 ml of this solution. The desired product was obtained by drop-wise addition of different concentration (0.0, 0.02, 0.04, 0.06 and 0.08 weight %) of dopant precursor into the main precursor. The step wise detail of synthesis process is given below.

Synthesis of undoped TiO_2

The mixture of 25 ml TTIP and 50 ml of ethanol was taken and the reaction was performed at room temperature with a magnetic stirrer with constant stirring, until a white gel is obtained. The prepared gel was dried for 10 hours and then crushed to get fine powder.

Synthesis of Ni-doped TiO_2 (0.02 weight %)

The mixture of 25 ml TTIP and 50 ml of ethanol was taken (main precursor) into a beaker and 6.82 ml of dopant precursor was added drop wise into the main precursor. The reaction was performed at room temperature under stirring until the gel of mixture was obtained. The prepared gel was dried for 10 hours and then crushed it to get fine powder.

Synthesis of Ni-doped TiO_2 (0.04 weight %)

The whole process was similar as mentioned in step 2, but 14 ml of dopant precursor was mixed drop wise into the main precursor for the reaction.

Synthesis of Ni-doped TiO_2 (0.06 weight %)

The whole process was similar to step 2, but 20.48 ml of dopant precursor was mixed drop wise into the main precursor for the reaction.

Synthesis of Ni-doped TiO_2 (0.08 weight %)

The whole process was similar to step 2, but 27.36 ml of dopant precursor was mixed drop wise into the main precursor for the reaction.

Characterizations

The prepared powder samples were calcinated for one hour in a box furnace at a temperature of 400°C. All the samples were characterized by the various techniques such as X-ray diffraction (XRD), scanning electron microscopy (SEM), Fourier transform infrared spectroscopy (FTIR), ultraviolet visible spectroscopy (UV-Vis), Raman spectroscopy, thermogravimetry analysis (TGA), photoluminescence spectroscopy (PL) and photoconductivity.

Results and discussion

X-ray diffraction

X-ray diffraction pattern of Ni-doped TiO_2 powders formed at 400°C for 1h are shown in **Fig. 1**. All the Ni-doped TiO_2 nanoparticles show anatase in phase (JCPDS 731764) and indicate that there is no other phase in the samples. The TiO_2 is stabilized in anatase phase after doping with Ni at lower levels can be attributed to the similar ionic radius of Ni^{+2} (0.72 A°) to that of Ti^{+4} (0.68 A°), which was found to replace some portion of Ti^{+4} ions in titania lattice **[15, 20, 24–29]**.

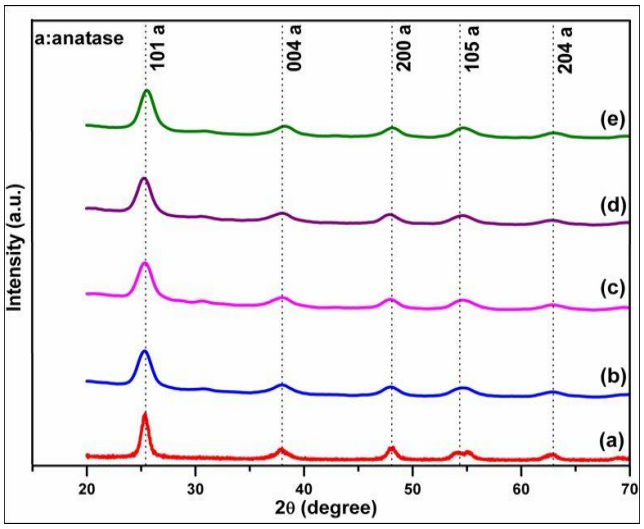

Fig. 1. XRD pattern of Ni doped TiO_2 nanoparticles annealed at 400°C (a) 0.0wt %, (b) 0.02wt%, (c) 0.04 wt%, (d) 0.06 wt% and (e) 0.08 wt%.

This suggest that Ni up to a concentration of 0.08% could replace some portion of Ti^{+4} ions in TiO_2 lattice or occupy interstitial positions of TiO_2 crystal structure or stay on the surface of TiO_2 as a single lamella of unimolecular oxide amorphous monolayer hence no XRD peaks corresponding to NiO or $NiTiO_3$ have been observed. The average crystallite size has been calculated by Scherer formula D = K λ/β cosθ where D is average crystallite size, K= 0.9, is the shape factor, λ is the wavelength of X-ray radiations, β is the full width at half maximum (FWHM) and θ is the diffraction angle. The X-ray density has been calculated for the samples by using equation (1) **[30-31]**:

$$\rho = \frac{nM}{NV} \tag{1}$$

where M is the molecular weight, N is Avogadro's number and V is the volume of unit cell. For anatase phase *n* is four and for rutile phase *n* is two **[32, 33]**. Further, the specific surface area is calculated by the formula **[31]**:

$$S_a = \frac{6}{D \times \rho} \tag{2}$$

where *D* is crystallite size and ρ is density. The density of all the samples is very close to each other. When dopant concentration was increased the crystallite size value decreases from 27.2 to 6.81 nm and the surface area increases from 56.7 to 225.6 m^2/ gram as shown in **Table 1**. These results suggest that Ni doping concentration effectively inhibits TiO_2 grain growth probably by staying at grain boundaries thereby decreasing the crystallite size and increasing the surface area **[15, 20, 24–29]**. The decrease in grain growth can also be attributed to the formation of Ni–O–Ti bonds in the doped powders, which inhibits the growth of the crystals. Using Williamson-Hall plot, the lattice strain has been calculated using the relation **[34]**:

$$\frac{\beta \cos\theta}{\lambda} = \frac{1}{\sigma} + \frac{\eta \sin\theta}{\lambda} \tag{3}$$

where β is FWHM in radians, λ is the wavelength of X-ray, θ is the diffraction angle, σ is the effective particle size and η is the effective strain.

Table 1. Structural parameters of Ni doped nanoparticles.

Calculated parameters	0.0 wt %	0.02 wt %	0.04 wt %	0.06 wt%	0.08 wt%
FWHM (degree)	0.2991	0.8974	1.1965	1.0470	1.0470
Lattice constant (Å)	a= b= 3.786 c= 9.504	a= b= 3.806 c= 9.476	a= b= 3.788 c= 9.456	a= b= 3.796 c= 9.448	a= b= 3.768 c= 9.384
d- spacing (Å)	3.5280	3.5275	3.5040	3.5071	3.4823
Unit cell volume a^2c (Å^3)	136.08	137.26	135.62	136.14	133.24
Average crystallite size (nm)	27.2	9.07	6.81	7.78	7.78
Density ρ (g/cm^3)	3.89	3.86	3.91	3.89	3.98
Specific surface area S_a (m^2/g)	56.7	171.3	225.6	198.3	193.5

Fig. 2 shows the Williamson-Hall plot between $\beta cos\theta/\lambda$ and $sin\theta/\lambda$ for the prepared samples. Negative slope in the plot indicates the presence of compressive strain **[35]** whereas the positive slope indicates the presence of tensile strain **[36]**. In this case, the prepared TiO_2 at different Ni proportions (0, 0.02, 0.04, 0.06, and 0.08) have positive slopes (Figure 2) which indicates the presence of tensile strain in the lattice of the samples. When compare to bulk anatase TiO_2 (a = b = 3.784Å and c = 9.514Å), a variation in lattice constants has been observed for the prepared samples as shown in Table 1, may be due to the tensile strain in the lattice. The shape and surface morphology of doped nano-powders have a critical role in the phase determination.

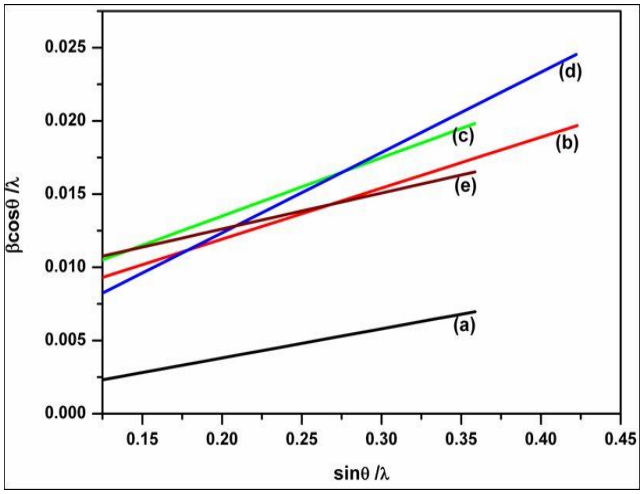

Fig. 2. Williamson-Hall plots of TiO_2 nanoparticles with different Ni content annealed at 400℃ (**a**) 0 wt %, (**b**) 0.02 wt %, (**c**) 0.04 wt %, (**d**) 0.06 wt % and (e) 0.08 wt %.

Field emission scanning electron microscope and transmission electron microscope

The FESEM image taken for Ni doped TiO_2 nanoparticle is shown in **Fig. 3**. It shows that at higher doping percentage the less agglomeration has occurred. The nanostructures exhibit interparticle aggregation, which is consistent with the morphology shown in the **Fig. 4** of TEM results. The TEM image of the samples shows the nanoparticles are spherical in shape. This is clear from the TEM image that as the concentration of Ni increases the particle size does not show any remarkable variation as the reaction time, temperature and other environmental conditions are maintained. The selected area electron diffraction (SAED) indicates that polycrystalline nature of the samples. It shows that the crystallinity decreases with increase in Ni content.

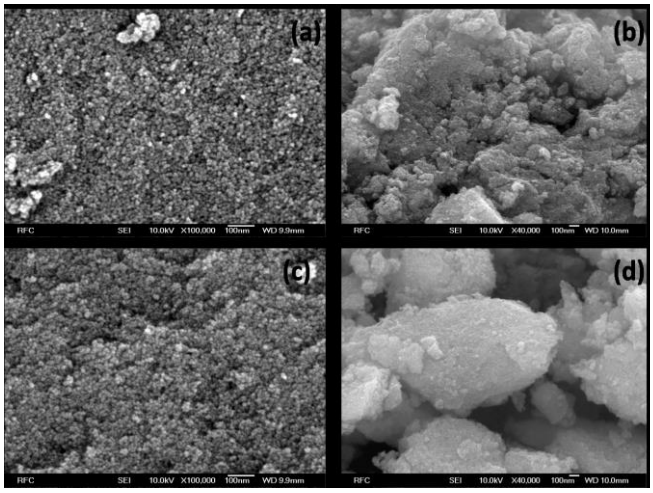

Fig. 3. FESEM image of prepared sample with different Ni content annealed at 400^0 C (a) 0.02 wt %, (b) 0.04 wt %, (c) 0.06 wt % and (d) 0.08 wt %.

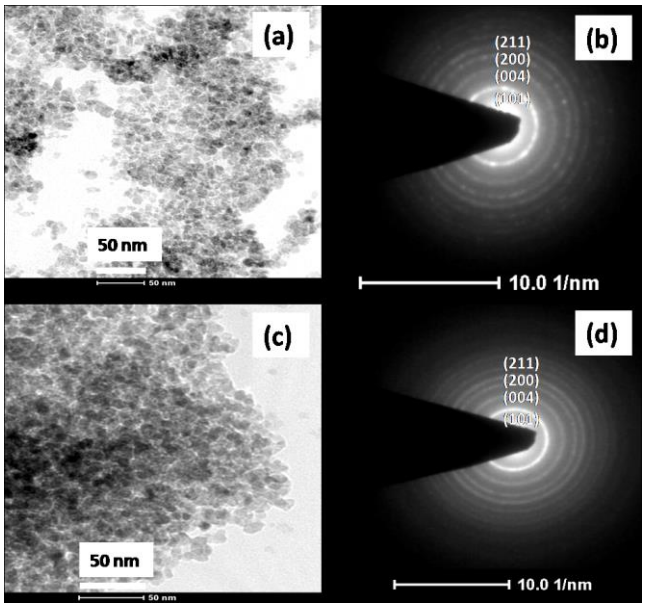

Fig. 4. TEM micrographs at the 50 nm scale of TiO_2 having Ni content: (a) 0.04 wt%, (b) 0.04 wt% SAED pattern, (c) 0.08 wt% and (d) 0.08 wt% SAED pattern.

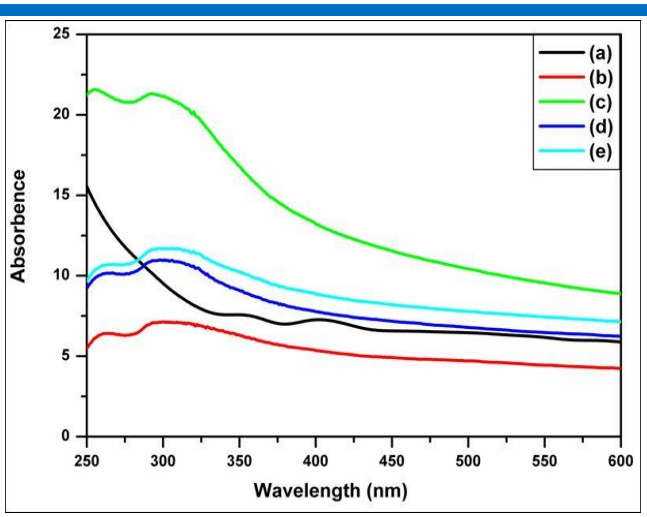

Fig. 5. UV-Vis absorption spectra of prepared samples with different Ni content annealed at 400℃ (a) 0 wt %, (b) 0.02 wt %, (c) 0.04 wt %, (d) 0.06 wt % and (e) 0.08 wt %.

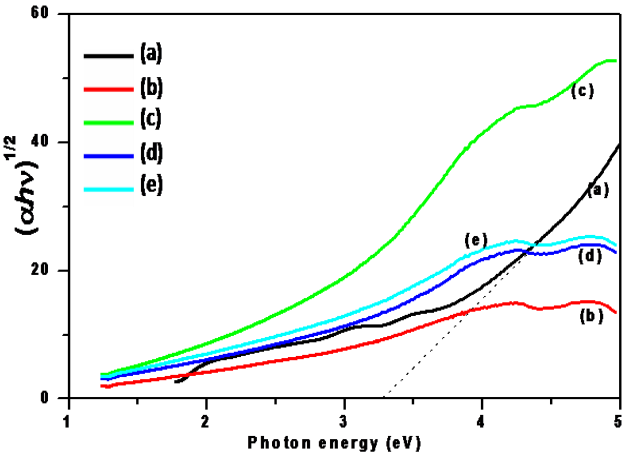

Fig. 6. Tauc plot of prepared samples with different Ni content annealed at 400℃ (a) 0 wt %, (b) 0.02 wt %, (c) 0.04 wt %, (d) 0.06 wt % and (e) 0.08 wt %.

UV-visible spectroscopy

The optical absorption spectra are depicted in **Fig. 5** and optical band gap energy is calculated by Tauc plots shown in **Fig. 6** for synthesized Ni doped TiO_2 nanoparticles. The absorption band gap energy can be determined by the following equation **[37-38]**.

$$(\alpha h\nu)^n = B(h\nu - E_g) \quad (4)$$

where $h\nu$ is the photon energy, α is the absorption coefficient, B is a constant relative to the material and n is a value that depends on the nature of transition (n=2 for direct band gap, 2/3 for direct forbidden gap and 1/2 for indirect band gap). The undoped TiO_2 sample (Figure 5.5 (a)) shows absorption at around 383 nm (3.24 eV) (i.e., in the UV range) which occurs due to the charge transfer from the valence band (mainly formed by 2p orbitals of the oxide anions) to the conduction band (mainly formed by 3d t_{2g} orbitals of the Ti^{4+} cations) **[39]**. The Ni-doped TiO_2 (Ni = 0.02, 0.04, 0.06, 0.08 weight %) having absorption bands in the wavelength range 465-586 nm (visible region) and band gap energy range 2.66-2.11eV have been observed and

calculated band gaps are shown in Table 2, which are due to the crystal field splitting of $3d^8$ orbital and due to charge transfer from Ni^{2+} to Ti^{4+} **[15]**. The doping of various transitional metal ions into TiO_2 shifts its optical absorption edge from UV into visible-light range (i.e., red shift) **[40]**. The absorption at wavelength greater than 425 nm affects the formation or recombination of electron-hole pairs and separation in a photocatalytic application under light radiation **[31]**.

Raman and FTIR spectra

The Raman spectra of Ni-doped TiO_2 are shown in **Fig. 7** and the Raman bands for pure TiO_2 are located at 147 cm^{-1} (E_g), 199 cm^{-1} (E_g), 399 cm^{-1} (B_{1g}), 518 cm^{-1} ($A_{1g}+B_{1g}$) and 643 cm^{-1} (E_g) **[41-42]**, indicating the presence of the anatase phase in un-doped TiO_2. The inset of **Fig. 7** represents the exact peak position (in cm^{-1}) corresponding to the highest intense peak for the un-doped and doped TiO_2 nanoparticles. The Raman spectra for Ni-doped TiO_2 nanoparticles indicate that the peaks of all doped samples shift towards the lower wave number (red shift) and no indication of the presence of rutile or any secondary phases are seen. Furthermore it is in agreement with XRD and UV-Vis absorption results.

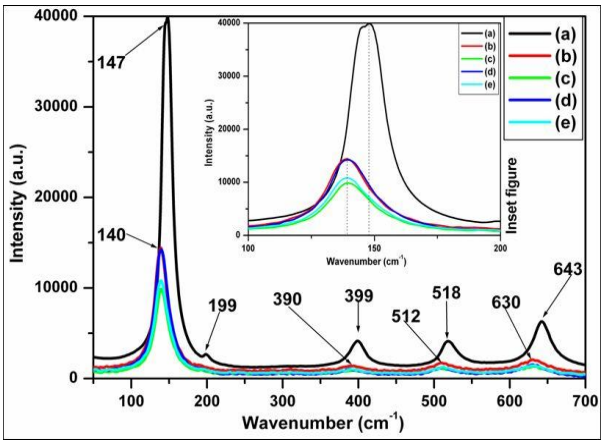

Fig. 7. Raman spectra of samples with different Ni proportions (a) 0 wt %, (b) 0.02 wt %, (c) 0.04 wt %, (d) 0.06 wt % and (e) 0.08 wt % annealed at 400°C. The inset shows the shifting towards lower wave number for highest intense peak in Raman bands.

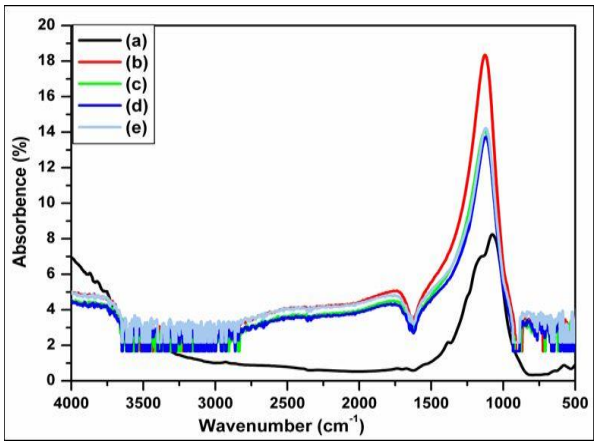

Fig. 8. FTIR spectra of samples with different Ni content annealed at 400°C (a) 0 wt %, (b) 0.02 wt %, (c) 0.04 wt % (d) 0.06 wt % and (e) 0.08 wt %.

Fig. 8 shows the FTIR spectra of synthesized samples. The absorption bands in the range of 400-800 cm^{-1} are mainly ascribed to Ti-O and Ti-O-O bonds **[42-45]**. The vibration is dominant in Ni doped samples (curves b, c, d and e) as compared to undoped sample (curve a). The vibrational band in the range of 1300 cm^{-1} to 4000 cm^{-1} mainly indicates the adsorbed H_2O and CO_2 molecules on the surface **[42]**. The broad intense band between 1200 cm^{-1} and 1022 cm^{-1} is present in all the samples which indicate the Ti-O-Ti vibrations **[42]**. The intensity of this band is higher in all the Ni doped samples as compared to pure TiO_2 sample which indicates more number of Ti-O-Ti vibrations in doped samples. The stretching vibration of the O-H and bending vibration of the adsorbed water molecules are also present (1620 cm^{-1} to 1630 cm^{-1}) in the Ni doped TiO_2 samples **[42]**.

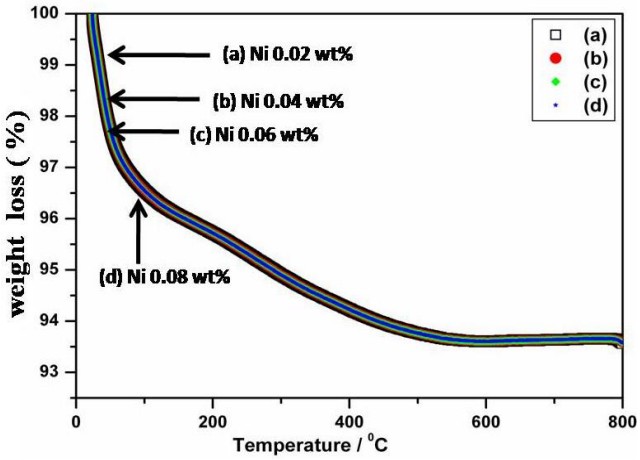

Fig. 9. TGA of samples with different Ni proportions annealed at 400°C (a) 0.02 wt %, (b) 0.04 wt %, (c) 0.06 wt % and (d) 0.08 wt %.

Thermogravimetry analysis

TGA profiles of prepared samples are represented in **Fig. 9**. The weight loss in the temperature range 90°C to 200°C is attributed to the loss of adsorbed water in the titanium oxide **[46]**. The combustion of residual organic species, including the dehydroxylation of the gel and decomposition of Cl ions are responsible for the loss in the range of 300 °C to 550 °C **[47]**. The weight loss of 6% for all the doped samples has been observed.

Photoluminescence spectroscopy

Fig. 10 illustrates the photoluminescence spectra of Ni doped TiO_2 nanoparticles. The PL spectra of prepared samples are obtained as a result of the competition among electron-hole separations, electron-phonon scattering and electron-hole recombination. TiO_2 has a direct band gap is subjected to dipole-forbidden transition **[48]**. PL spectra of anatase TiO_2 materials are attributed to three kinds of physical origins: self-trapped excitons **[59-50]**, oxygen vacancies **[50-51]** and surface states (defects) **[52]**. Most of the surface states are oxygen vacancies or the Ti^{4+} ions adjacent to oxygen vacancies **[53-54]**. PL measurement of pure TiO_2 nanoparticles show clear emission bands (**Fig. 10 (c)**). The blue-green emission of 485 nm (~2.55 eV) in TiO_2 and 480 nm (~2.58 eV) in Ni-doped TiO_2 for Ni concentration of 0.02, 0.04, 0.08 wt% has been observed.

This can be attributed to the charge transfer from Ti^{3+} to oxygen anion in a $[TiO_6]^{8-}$ complex associated with oxygen vacancies at the surface, indicating the band is originating from the intrinsic state rather than the surface state. In doped TiO_2 for Ni content of 0.02, 0.04, 0.08 wt% this emission edge is 0.03 eV below to the TiO_2, but for Ni content of 0.06 wt% the emission peak of 436 nm (~ 2.84 eV) has been observed which is 0.07 eV below to blue emission edge of 447 nm (~ 2.77eV) (**Fig. 10 b**). The visible emission was also observed in PL spectra of for doped samples which are attributed to the oxygen vacancies and Ti vacancies introduced after Ni doping.

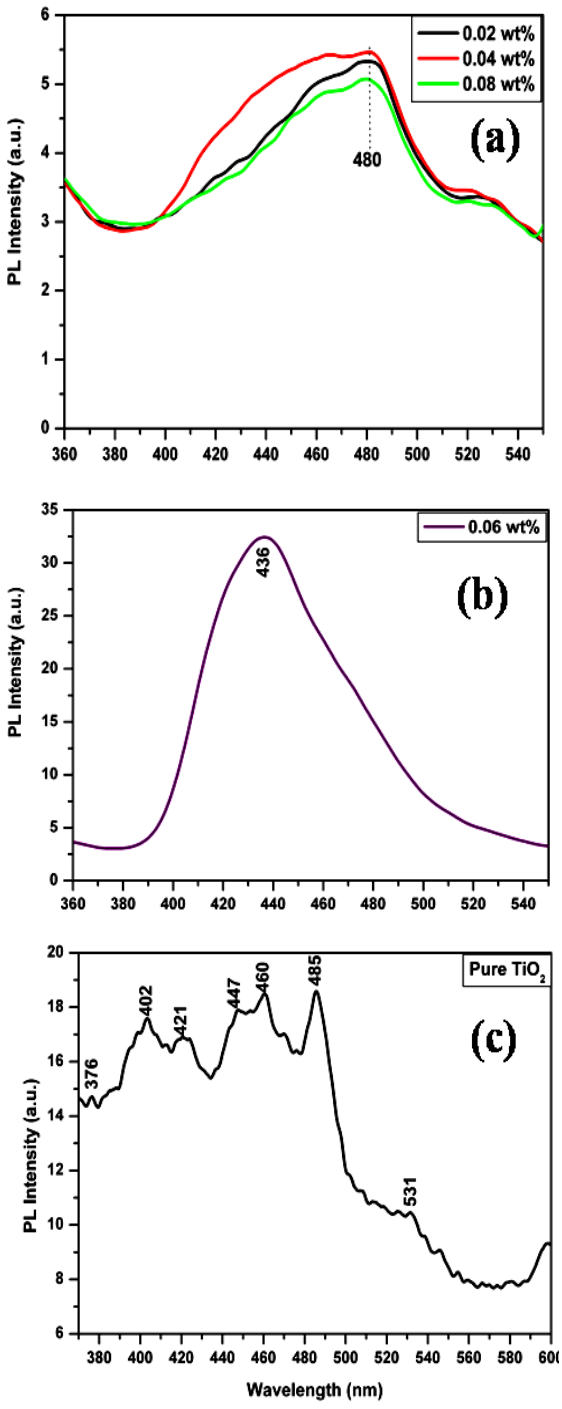

Fig. 10. Photoluminescence spectrum (PL) of prepared samples with different Ni content annealed at 400°C (a) 0.02, 0.04 and 0.08 wt %, (b) 0.06 wt % and (c) Pure TiO_2.

Photoconductivity measurements

The rise and decay time transient photoconductivity response measurements help to study the photoconductivity dynamics of TiO_2 nanoparticles during which the light was abruptly switched on and off at room temperature. The time-resolved rise and decay of the photocurrent spectra for the Ni doped TiO_2 nanoparticles under visible illumination of 370 nm are shown in **Fig. 11**.

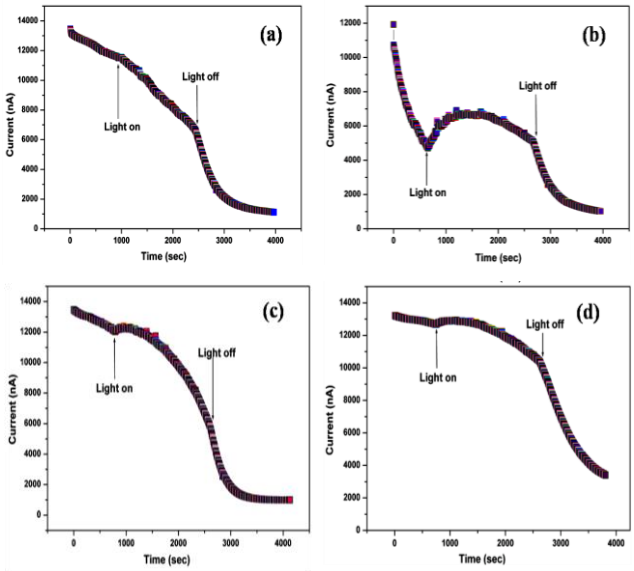

Fig. 11. Photoconductivity (PC) rise and decay time spectra: photoconductive response due to visible light excitation for TiO_2 nanoparticles containing Ni weight percentage of (a) 0.02, (b) 0.04, (c) 0.06 and (d) 0.08 wt %.

The surface related phenomenon, which is primarily governed by adsorption and desorption processes, plays an important role in the photoconductivity properties of the nanostructures due to large surface-to-volume ratio **[55]**. The rise and decay of photocurrent spectra is useful in determining the nature of trap and recombination centers present inside the materials. When the field is applied, the initial dark current is very high in prepared samples. This may be attributed due to the presence of oxygen vacancies at the surface and other native defects acting as donors as well as the process of the adsorption of water molecules, thereby releasing charge carriers. After it the dark current starts decreasing and attains a minimum value in all the samples. When visible illumination is switched on, the photocurrent rises in the samples, but this rise in photocurrent is high in TiO_2 as compared to Ni doped TiO_2 nanoparticles. When illumination is switched off, electron−hole recombination process dominates, so the conductivity decreases in the samples. Slow photoconductive rise and decay response may be attributed to a large amount of recombination centers and presence of trap levels and defect states within the band gap **[56-61]**.

Trap depth is defined as the required energy to remove an atom from the trap. Trap depths can be calculated from decay curves. According to Bube model the decay of photocurrent can be represented by the equation $I = I_0 \exp(-pt)$, **[58]**, where I_0 is the current at the time when light is switched off, I is photocurrent at any instant of time for growth and decay function and probability of escape of an

electron from trap per second is $p = S \exp(-E/kT)$. The trap depth (E) can be calculated by using the following equation:

$$E = kT\left[\ln S - \ln \frac{\ln \frac{I_o}{I}}{t}\right] \quad (5)$$

where E denotes trap depth, k is Boltzmann constant, T is the absolute temperature and S is the frequency factor **[31]** defined as the number per second that the quanta from the lattice vibrations (phonons) attempt to eject the electron from the trap multiplied by the probability of transition of the ejected electron to the conduction band of the order of 10^9 at room temperature. Here the trap depth calculated for TiO_2 is 0.67 eV, while the trap depths are 0.67eV, 0.67eV, 0.66eV, 0.70eV obtained for TiO_2 containing Ni weight percentage 0.02, 0.04, 0.06, 0.08 respectively. These values are much greater than the reported values for anatase TiO_2 between 0.10 and 0.27 eV **[59-60]**.

Conclusion

The Ni doped titania nanostructures were synthesized by sol-gel method and calcinated at 400°C are discussed in detail. The synthesized materials were characterized by XRD, SEM, TEM, UV-Vis, PL and photoconductivity measurements. The Ni-doped TiO_2 nanoparticles are anatase in phase with no other additional impurity phase in the samples. The XRD result shows that the average crystallite size decreases with increase in Ni proportions in TiO_2 which is consistent with the morphology observed by SEM and TEM images. All the Ni doped TiO_2 nanoparticles are spherical in shape and exhibit anatase phase with tensile strain in the host. The nanostructures exhibit interparticle aggregation. The optical band gap of doped TiO_2 nanostructures indicates the red shift with blue-green emission bands while the undoped TiO_2 exhibits possible emission bands. XRD spectra confirm that Ti atom has been successfully replaced by Ni atom in all the samples and it is not present on the surface in the metal-oxide form. Thus depending on the nature of chemical dopant the adsorption of visible light in titania lattice can be tuned easily. The emissions observed in PL spectra of all the doped samples are attributed to the oxygen vacancies and Ti vacancies introduced after Ni doping. The synthesized TiO_2 exhibits enhanced photoconductivity properties. The observed trap depth value is greater in the samples than the previously published results on TiO_2 nanoparticles. The present work suggest that semiconducting oxide materials can have potential applications in optoelectronic devices such as solar cells, photoconductors in replacement of expansive materials by fine controlling of the compositions and morphology in the oxide materials.

Acknowledgements

The authors are thankful Director MNNIT for providing the characterization facility and funding support through TEQIP-II project for carrying out the research work. One of the authors is thankful to Prof. R. K. Shukla, Lucknow University for PL, PC facilities and their valuable discussion for the research work.

Reference

1. Nada, A. A.; Hamed, H. A.; Barakat, M. H.; Mohamed, N. R.; Veziroglu, T. N.; *Intern. J. Hydrogen Energy*, **2008**, *33*, 3264. **DOI:** 10.1016/j.ijhydene.2008.04.027.
2. Jing, D.; Zhang, Y.; Guo, L.; *Chem. Phys. Lett*., **2005**, *415*, 74. **DOI:** 10.1016/j.cplett.2005.08.080.
3. On, D. T.; Giscard, D. D.; Kaliaguine, D. S.; *Appl. Catal. A*, **2003**, *253*, 545. **DOI:** 10.1016/S0926-860X(03)00195-9.
4. Zeng, P.; Zhang, X.; Zhang, X.; Chai, B.; Peng, T.; *Chem. Phys. Lett.*, **2011**,*503*, 262. **DOI:** 10.1016/j.cplett.2011.01.007.
5. Tripathi, A. K.; Mathpal, M. C.; Kumar, P.; Singh, M. K.; Soler, M. A. G.; Agarwal, A.; Journal of Alloys and Compounds, **2015**, *622*, 37. **DOI:** 10.1016/j.jallcom.2014.09.218.
6. In, S. I.; Vesborg, P. C. K.; Abrams, B. L.; Hou, Y.; Chorkendorff, I.; *J. Photochem. Photobiol. A: Chem*, **2011**, *222*, 258. **DOI:** 10.1016/j.jphotochem.2011.06.005.
7. Mathpal, M. C.; Tripathi, A. K.; Kumar, P.; Agrahari, V.; Singh, M. K.; Agarwal, A.; *Chem. Phys. Lett*. **2014**, *614*, 162. **DOI:** 10.1016/j.cplett.2014.09.035.
8. Asahi, R.; Morikawa, T.; Ohwaki, T.; Aoki, K.; Taga, Y.; *Science*, **2001**, *293*, 269. **DOI:** 10.1126/science.1061051.
9. Kudo, A.; Sekizawa, M.; *Chem. Commun*., **2000**, *15*, 1371. **DOI:** 10.1039/B003297M.
10. Sreethawong, T.; Suzuki, Y.; Yoshikawa, S.; *Int. J. Hydrogen Energy*, **2005**, *30*, 1053. **DOI:** 10.1016/j.ijhydene.2004.09.007.
11. Bak, T.; Nowotny, J.; Rekas, M.; Sorrell, C. C.; *Int. J. Hydrogen Energy*, **2002**, *27*, 991. **DOI:** 10.1016/S0360-3199(02)00022-8.
12. Gole, J. L.; Prokes, S. M.; Glembocki, O. J.; Wang, J.; Qiu, X.; Burda, C.; *Nanoscale*, **2010**, *2*, 1134. **DOI:** 10.1039/c0nr00125b.
13. Hamadanian, M.; Reisi-Vanani, A.; Majedi, A.; *Journal of the Iranian Chemical Society*, **2010**, *7*, S52. **DOI:** 10.1007/BF03246184.
14. Subramanian, M.; Vijayalakshmi, S.; Venkataraj, S.; Jayavel, R.; *Thin Solid Films*, **2008**, *516*, 3776. **DOI:** 10.1016/j.tsf.2007.06.125.
15. Lin, Y. J.; Chang, Y. H.; Yang, W. D.; Tsai, B. S.; *Journal of Non-Crystalline Solids* **2006**, *352*, 789. **DOI:** 10.1016/j.jnoncrysol.2006.02.001.
16. Ganesh, I.; Kumar, P. P.; Gupta, A. K.; Sekhar, P. S. C.; Radha, K.; Padmanabham, G.; Sundararajan, G.; *Processing and Application of Ceramics*, **2012**, *6*, 21. **DOI:** 10.2298/PAC1201021G.
17. I. Ganesh, P. P. Kumar, A. K. Gupta, P. S.C. Sekhar, K. Radha, G. Padmanabham, G. Sundararajan, *Mater. Chem. Phys.* **2012**, *135*, 220. **DOI:** 10.1016/j.matchemphys.2012.04.062.
18. Gracien, E. B.; Shen, J.; Sun, X., Liu, D.; Li, M.; Yao, S.; Sun, J.; *Thin Solid Films*, **2007**, *515*, 5287. **DOI:** 10.1016/j.tsf.2006.12.187.
19. De haart, L. G. J.; De vries, A. J.; Blasse, G.; *Materials Research Bulletin*, **1984**, *19*, 817. **DOI:** 10.1016/0025-5408(84)90042-4.
20. Begum, N. S.; Ahmed, H. M. F.; Gunashekar, K. R.; *Bulletin of Materials Science* **2008**, *31*, 747. **DOI:** 10.1007/s12034-008-0118-x.
21. Sreethawong, T.; Suzuki, Y.; Yoshikawa, S.; *Int. J. Hydrogen Energy*, **2005**, *30*, 1053. **DOI:** 10.1016/j.ijhydene.2004.09.007
22. Wang, Y.; Hao, Y.; Cheng, H.; Ma, J.; Xu, B.; Li, W.; Cai, S.; *J. Mater. Sci.* **1999**, *34*, 2773. **DOI:** 10.1023/A:1004658629133.
23. Devi, L. G.; Kottam, N.; Kumar, S. G.; Rajashekhar, K. E.; *Centr. Europ. J. Chem.* **2010**, *8*, 142. **DOI:** 10.2478/s11532-009-0115-y.
24. Shu, X.; He, J.; Chen, D.; *Ind. Eng. Chem. Res.* **2008**, *47*, 4750. **DOI:** 10.1021/ie071619d.
25. Kim, D. H.; Park, H. S.; Kim, S. J.; Lee, K. S.; *Cat. Lett.* **2006**,*106*, 29. **DOI:** 10.1007/s10562-005-9186-3.

26. Sadjadi, M. S.; Mozaffari, M.; Enhessari, M.; Zare, K.; *Superlattices and Microstructures*, **2010**, *47*, 685. **DOI:** 10.1016/j.spmi.2010.02.007.
27. Witke, K.; Brzezinka, K. W.; Reich P.; *Fresenius' J. Analyt. Chem.* **1998**, *361*, 619. **DOI:** 10.1007/s002160050969.
28. Chuang, S.-H.; Hsieh, M.-L.; Wu, S.-C.; Lin, H.-C.; Chao, T.-S.; Hou, T.-H.; *J. Am. Ceram. Soc.* **2011**, *94*, 250. **DOI:** 10.1111/j.1551-2916.2010.04037.x.
29. Lopes, K. P.; Cavalcante, L. S.; Sim˜oes, A. Z.; Varela, J. A.; Longo, E.; Leite, E. R.; *J. Alloy. Comp.* **2009**, *468*, 327. **DOI:** 10.1016/j.jallcom.2007.12.085.
30. Tripathi, A. K.; Mathpal, M. C.; Kumar, P.; Singh, M. K.; Mishra, S. K.; Srivastava, R. K.; Chung, J. S.; Verma, G.; Ahmad, M. M.; Agarwal, A.; *Mat. Sci. Semicond. Proc.* **2014**, *23*, 136. **DOI:** 10.1016/j.mssp.2014.02.041.
31. Maurya, A.; Chauhan, P.; Mishra, S. K.; Srivastava, R.K.; *J. Alloys and Comp*, **2011**, *509*, 8433. **DOI:** 10.1016/j.jallcom.2011.05.108.
32. Kingon, A. I.; Maris, J. P.; Steiffer, S. K.; *Nature*, **2000**, *406*, 1032. **DOI:** 10.1038/35023243.
33. Li, W.; Ni, C.; Lin, H.; Huang, C. P.; Shah, S. I.; *J. Appl. Phys.* **2004**, *96*, 6663. **DOI:** 10.1063/1.1807520.
34. Williamson, G. K.; Hall, W. H.; *Acta Metal*, **1953**, *1*, 22. **DOI:** 10.1016/0001-6160(53)90006-6.
35. Prabhu, R. R.; Abdul Khadar, M.; *Bull. Mater. Sci*, **2008**, *31*, 511. **DOI:** 10.1007/s12034-008-0080-7.
36. Kumar, S.; Vickraman, P.; Jayachandran, M.; *J. Mater. Sci. Mater. Electron*, **2010**, *21*, 343. **DOI:** 10.1007/s10854-009-9918-z.
37. Salem, A. M.; Soliman Selim, M.; *J. Phys, D: Appl. Phys*, **2001**, *34*, 12. **DOI:** 10.1088/0022-3727/34/1/303.
38. Mathpal, M. C.; Tripathi, A. K.; Kumar, P.; Balasubramaniyan, R.,; Singh, M. K.; Chung, J. S.; Hur, S. H.; Agarwal, A.; *Phys. Chem. Chem. Phys.* **2014**, *16*, 23874. **DOI:** 10.1039/C4CP02982H.
39. Venkatachalam, N.; Palanichamy, M.; Murugesan, V.; *Mater. Chem. Phys.* **2007**, *104*, 454. **DOI:** 10.1016/j.matchemphys.2007.04.003.
40. Wu, J. C. S.; Chen, C. H.; *J. Photochem. Photobiol. A*, **2004**, *163*, 509. **DOI:** 10.1016/j.jphotochem.2004.02.007.
41. Krishnamurti, D.; *Ind. Acad. Sci.* **1962**, *55*, 290. **DOI:** 10.1007/BF03045870.
42. Swamy, V.; Muddle, B.C.; Dai, Q.; *Appl. Phys. Lett*, **2006**, *89*, 163118 (1-3). **DOI:** 10.1063/1.2364123.
43. Rath, C.; Mohanty, P.; Pandey, A. C.; Mishra, N. C.; *J. Phys. D: Appl. Phys*, **2009**, 42, 205101. **DOI:** 10.1088/0022-3727/42/20/205101.
44. Choi, H. C.; Jung, Y. M.; Kim, S. B.; *Vib. Spectrosc*, **2005**, *37*, 33. **DOI:** 10.1016/j.vibspec.2004.05.006.
45. Seok, S.; Kim, J. H.; *Mat. Chem. and Phys*, **2004**, *86*, 176. **DOI:** 10.1016/j.matchemphys.2004.02.020.
46. Sonawane, R. S.; Kale, B. B.; Dongare, M. K.; *Mater. Chem. Phys*, **2004**, *85*, 52. **DOI:** 10.1016/j.matchemphys.2003.12.007.
47. Hung, W. C.; Chen, Y. C.; Chu, H.; Tseng, T. K.; *Appl. Surf. Sci*, **2008**, *255*, 2205. **DOI:** 10.1016/j.apsusc.2008.07.079
48. Zou, B.; Xiao, L.; Li, T.; Zhao, J.; Lai, Z.; Gu, S.; *Appl. Phys. Lett*, **1991**, *59*, 1826. **DOI:** 10.1063/1.352766
49. Tang, H.; Berger, H.; Schmid, P. E.; Levy, F.; **1993**, *87*, 847. **DOI:** 10.1016/0038-1098(93)90427-O.
50. Saraf, L. V.; Patil, S. I.; Ogale, S. B.; Sainker, S. R.; Kshirsager, S. T.; *Int. J. Mod. Phys. B*, **1998**, *12*, 2635. **DOI:** 10.1142/S0217979298001538.
51. Serpone, N.; Lawless, D.; Khairutdinov, R.; *J. phys. Chem*, **1995**, *99*, 16646. **DOI:** 10.1021/j100045a026.
52. Forss, L.; Schubnell, M.; *Appl. Phys. B*, **1993**, *56*, 363. **DOI:** 10.1007/BF00324533.
53. Redmond, G.; Fitzmaurice, D.; Graetzel, M.; *J. Phys. Chem*, **1993**, *97*, 6951. **DOI:** 10.1021/j100129a005.
54. Lu, G.; Linsebigler, A.; Yates, J. T.; *J. Phys. Chem*, **1994**, *98*, 11733. **DOI:** 10.1021/j100096a017.
55. Jie, J. S.; Zhang, W. H.; Jiang, Y.; Meng, X. M.; Lie, Y. Q.; Lee, S. T.; *Nano Lett*, **2006**, *6*, 1887. **DOI:** 10.1021/nl060867g.
56. Murphy, T. E.; Moazzami, K.; Phillips, J. D.; *J. Electron. Mater*, **2006**, *35*, 543. **DOI:** 10.1007/s11664-006-0097-x.
57. S.K. Mishral, R.K. Srivastava1, S.G. Prakash1, R.S. Yadav, A.C. Panday, *Opto. Electron. Rev.* **2010**, *18*, 467. **DOI:** 10.2478/s11772−010−0037−4.
58. R. H. Bube, Photoconductivity of solids, book published by John Wiley, New York, **1960**.
59. Boschloo, G.; Hagfeldt, A.; *J. Phys Chem. B*, **2005**, *109*, 12093. **DOI:** 10.1021/jp0513770
60. Cernea, M.; Secu, M.; Secu, C. E.; Baibarac, M.; Vasile, B. S.; *J. Nanopart. Res*, **2011**, *13*, 77. **DOI:** 10.1007/s11051-010-0002-7.
61. Agrahari,V.; Mathpal, M. C.; Kumar, M.; Agarwal, A.; *J. Alloys Comp.* **2015**, *622*, 48. **DOI:** 10.1016/j.jallcom.2014.10.009.